A Collider Search for Dark Matter Produced in Association with a Higgs Boson with the CMS Detector at the 13 TeV LHC

By

Dustin Ray Burns
B.S. (Georgia Institute of Technology) 2011
M.S. (University of California, Davis) 2012

Dissertation

Submitted in partial satisfaction of the requirements for the degree of

Doctor of Philosophy

in

Physics

in the

Office of Graduate Studies

of the

University of California

Davis

Approved:

Chair Michael Mulhearn

Robin Erbacher

Albert De Roeck

Committee in Charge

2017

Contents

List of Figures

List of Tables

Chapter 1

Datasets and Monte Carlo Simulations

1.1 Data

1.1.1 Triggers and Datasets

This analysis uses a data sample recorded by the CMS experiment during 2016, corresponding to 35.9 fb^{-1} of data. The datasets are listed in Table 1.1, along with the integrated luminosity. The analysis relies on five different primary datasets (PDs), *DoubleEG*, *DoubleMuon*, *MuEG*, *SingleElectron*, and *SingleMuon*, each of which combines a certain collection of HLT paths. To avoid duplicate events from different primary datasets, events are taken:

- from DoubleEG if they pass the diEle or triEle triggers,
- from DoubleMuon if they pass the diMuon or triMuon triggers and fail the diEle and triEle triggers,
- from MuEG if they pass the MuEle or MuDiEle or DiMuEle triggers and fail the diEle, triEle, diMuon and triMuon triggers,
- from SingleElectron if they pass the singleElectron trigger and fail all the above triggers.
- from SingleMuon if they pass the singleMuon trigger and fail all the above triggers.

The HLT paths used for 2016 collision data are listed in Table 1.2, together with their L1 seed, prescale value and the associated primary dataset.

Run-range	Dataset	Integrated luminosity
273150-275376	/DoubleMuon/Run2016B-23Sep2016-v3/AOD /DoubleEG/Run2016B-23Sep2016-v3/AOD /MuonEG/Run2016B-23Sep2016-v3/AOD /SingleElectron/Run2016B-23Sep2016-v3/AOD /SingleMuon/Run2016B-23Sep2016-v3/AOD	5.892 fb^{-1}
275656-276283	/DoubleMuon/Run2016C-23Sep2016-v1/AOD /DoubleEG/Run2016C-23Sep2016-v1/AOD /MuonEG/Run2016C-23Sep2016-v1/AOD /SingleElectron/Run2016C-23Sep2016-v1/AOD /SingleMuon/Run2016C-23Sep2016-v1/AOD	2.646 fb^{-1}
276315-276811	/DoubleMuon/Run2016D-23Sep2016-v1/AOD /DoubleEG/Run2016D-23Sep2016-v1/AOD /MuonEG/Run2016D-23Sep2016-v1/AOD /SingleElectron/Run2016D-23Sep2016-v1/AOD /SingleMuon/Run2016D-23Sep2016-v1/AOD	4.353 fb^{-1}
276831-277420	/DoubleMuon/Run2016E-23Sep2016-v1/AOD /DoubleEG/Run2016E-23Sep2016-v1/AOD /MuonEG/Run2016E-23Sep2016-v1/AOD /SingleElectron/Run2016E-23Sep2016-v1/AOD /SingleMuon/Run2016E-23Sep2016-v1/AOD	4.117 fb^{-1}
277932-278808	/DoubleMuon/Run2016F-23Sep2016-v1/AOD /DoubleEG/Run2016F-23Sep2016-v1/AOD /MuonEG/Run2016F-23Sep2016-v1/AOD /SingleElectron/Run2016F-23Sep2016-v1/AOD /SingleMuon/Run2016F-23Sep2016-v1/AOD	3.186 fb^{-1}
278820-280385	/DoubleMuon/Run2016G-23Sep2016-v1/AOD /DoubleEG/Run2016G-23Sep2016-v1/AOD /MuonEG/Run2016G-23Sep2016-v1/AOD /SingleElectron/Run2016G-23Sep2016-v1/AOD /SingleMuon/Run2016G-23Sep2016-v1/AOD	7.721 fb^{-1}
281207-284068	/DoubleMuon/Run2016H-PromptReco-v1/AOD /DoubleEG/Run2016H-PromptReco-v1/AOD /MuonEG/Run2016H-PromptReco-v1/AOD /SingleElectron/Run2016H-PromptReco-v1/AOD /SingleMuon/Run2016H-PromptReco-v1/AOD /DoubleMuon/Run2016H-PromptReco-v2/AOD /DoubleEG/Run2016H-PromptReco-v2/AOD /MuonEG/Run2016H-PromptReco-v2/AOD /SingleElectron/Run2016H-PromptReco-v2/AOD /SingleMuon/Run2016H-PromptReco-v2/AOD /DoubleMuon/Run2016H-PromptReco-v3/AOD /DoubleEG/Run2016H-PromptReco-v3/AOD /MuonEG/Run2016H-PromptReco-v3/AOD /SingleElectron/Run2016H-PromptReco-v3/AOD /SingleMuon/Run2016H-PromptReco-v3/AOD	8.857 fb^{-1}

Table 1.1: Datasets used in the analysis.

HLT path	L1 seed	prescale	primary dataset
HLT_Ele17_Ele12_CaloIdL_TrackIdL_IsoVL_DZ	L1_DoubleEG_15_10	1	DoubleEG
HLT_Ele23_Ele12_CaloIdL_TrackIdL_IsoVL_DZ	L1_DoubleEG_22_10	1	DoubleEG
HLT_DoubleEle33_CaloIdL_GsfTrkIdVL	(Multiple)	1	DoubleEG
HLT_Ele16_Ele12_Ele8_CaloIdL_TrackIdL	L1_TripleEG_14_10_8	1	DoubleEG
HLT_Mu17_TrkIsoVVL_Mu8_TrkIsoVVL	L1_DoubleMu_11_4	1	DoubleMuon
HLT_Mu17_TrkIsoVVL_TkMu8_TrkIsoVVL	L1_DoubleMu_11_4	1	DoubleMuon
HLT_TripleMu_12_10_5	L1_TripleMu_5_5_3	1	DoubleMuon
HLT_Mu8_TrkIsoVVL_Ele17_CaloIdL_TrackIdL_IsoVL	L1_Mu5_EG15	1	MuonEG
HLT_Mu8_TrkIsoVVL_Ele23_CaloIdL_TrackIdL_IsoVL	L1_Mu5_EG20	1	MuonEG
HLT_Mu17_TrkIsoVVL_Ele12_CaloIdL_TrackIdL_IsoVL	L1_Mu12_EG10	1	MuonEG
HLT_Mu23_TrkIsoVVL_Ele12_CaloIdL_TrackIdL_IsoVL	L1_Mu20_EG10	1	MuonEG
HLT_Mu23_TrkIsoVVL_Ele8_CaloIdL_TrackIdL_IsoVL	L1_SingleMu*	1	MuonEG
HLT_Mu8_DiEle12_CaloIdL_TrackIdL	L1_Mu6_DoubleEG10	1	MuonEG
HLT_DiMu9_Ele9_CaloIdL_TrackIdL	L1_DoubleMu7_EG7	1	MuonEG
HLT_Ele25_eta2p1_WPTight	L1_SingleEG*	1	SingleElectron
HLT_Ele27_WPTight	L1_SingleEG*	1	SingleElectron
HLT_Ele27_eta2p1_WPLoose_Gsf	L1_SingleEG*	1	SingleElectron
HLT_IsoMu20 OR HLT_IsoTkMu20	L1_SingleMu*	1	SingleMuon
HLT_IsoMu22 OR HLT_IsoTkMu22	L1_SingleMu*	1	SingleMuon

Table 1.2: Trigger paths used in 2016 collision data.

1.1.2 Trigger Efficiency

The efficiency in data of the combination of triggers used in the anlysis with respect to the offline reconstruction and selection is measured by considering 4ℓ events triggered by single lepton triggers. One of the four reconstructed leptons (the "tag") is geometrically matched to a trigger object passing the final filter of one of the single muon or single electron triggers. The other three leptons are used as "probes". In each 4ℓ event there are up to 4 possible tag-probe combinations, and all possible combinations are counted in the denominator of the efficiency. For each of the three probe leptons all matching trigger filter objects are collected. Then the matched trigger filter objects of the three probe leptons are combined in attempt to reconstruct any of the triggers used in the anlysis. If any of the analysis triggers can be formed using the probe leptons, the set of probes is also counted in the numerator of the efficiency.

This method does not have a perfect closure in MC events due to the fact that the presence of a fourth lepton increases the trigger efficiency, and this effect is not accounted for. Also, in the $2e2\mu$ final state, the three probe leptons cannot be combined to form all possible triggers which can collect events with two electrons and two muons (e.g. if the tag lepton is an electron, the three remaining leptons cannot pass a double electron trigger). Therefore the method is also exercised on MC and the difference between data

and MC is used to determine the reliability of the simulation. The efficiency plotted as a function of the minimum p_{T} of the three probe leptons in data and MC using this method can be seen in Fig.1.1. The MC efficiency describes well the data within the statistical uncertainties.

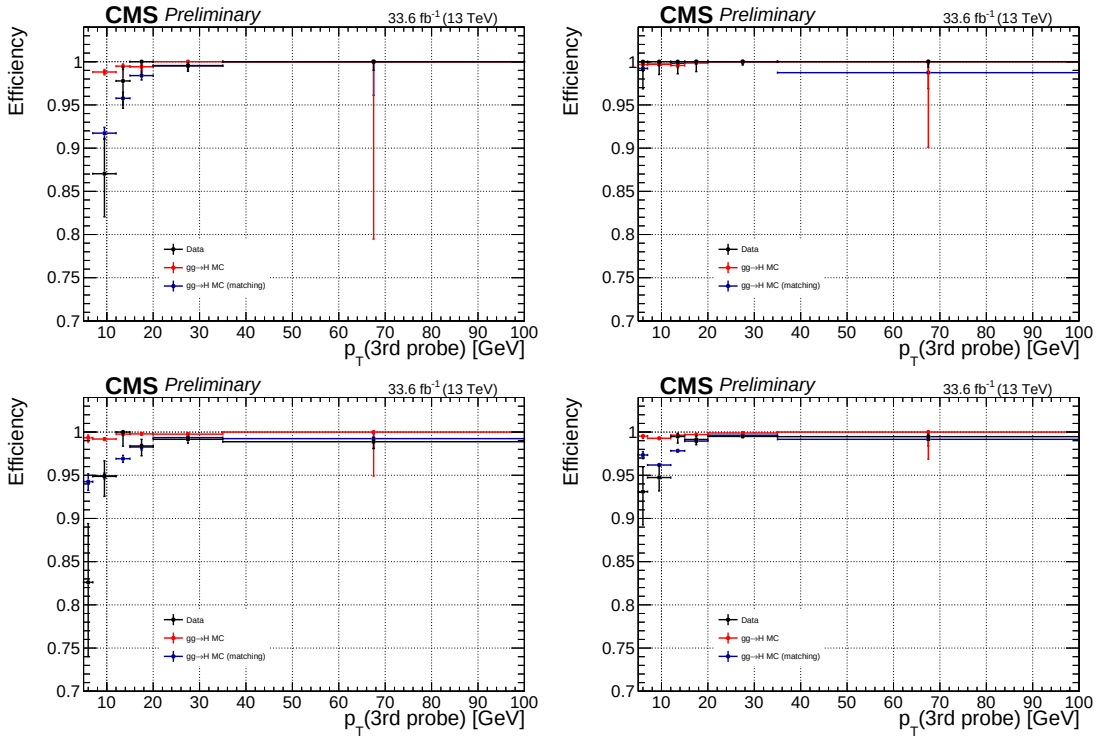

Figure 1.1: Trigger efficiency measured in data using 4ℓ events collected by single lepton triggers for the $4e$ (top left), 4μ (top right), $2e2\mu$ (bottom left) and 4ℓ (bottom right) final states.

A summary of the trigger efficiencies in MC truth, and in MC and data using the tag and probe method are summarized in table 1.3. The trigger efficiency in simulation is found to be $> 99\%$ in each final state.

1.2 Simulation

1.2.1 Signal Samples

The signal samples used are centrally produced for the benchmarks defined in the previous section and are summarized in Table 1.4.

Final State	$gg \to H$ MC	$gg \to H$ MC (matching)	Data (matching)
$4e$	$0.991^{+.002}_{-0.002}$	$0.948^{+.004}_{-0.004}$	$0.982^{+.005}_{-0.007}$
4μ	$0.997^{+.001}_{-0.001}$	$0.997^{+.001}_{-0.001}$	$1.000^{+.000}_{-0.001}$
$2e2\mu$	$0.995^{+.001}_{-0.001}$	$0.964^{+.002}_{-0.002}$	$0.983^{+.003}_{-0.004}$

Table 1.3: Trigger efficiencies measured using 4ℓ events.

Dataset	Parameters
/ZprimeToA0hToA0chichihZZTo4l_2HDM_MZp-*_MA0-300_13TeV-madgraph-pythia8/[1]	$m_{A^0} = 300$ GeV
/ZprimeToA0hToA0chichihZZTo4l_2HDM_MZp-*_MA0-*_13TeV-madgraph/[2]	$m_{A^0} \neq 300$ GeV
/MonoHZZ4l_ZpBaryonic_MZp-*_MChi-*_13TeV-madgraph/[3]	
[1] RunIISpring16DR80-premix_withHLT_80X_mcRun2_asymptotic_v14-v1/AODSIM	
[2] RunIISpring16reHLT80-PUSpring16RAWAODSIM_reHLT_80X_mcRun2_asymptotic_v14-v1/AODSIM	
[3] RunIISpring16DR80-premix_withHLT_80X_mcRun2_asymptotic_v14-v1/AODSIM	

Table 1.4: Benchmark signal samples analyzed.

1.2.2 Background Samples

Descriptions of the SM Higgs boson production are obtained using the POWHEG V2 [1, 2, 3] generator for the five main production modes: gluon fusion ($gg \to H$) including quark mass effects [4], vector boson fusion (VBF) [5], and associated production (WH, ZH and $t\bar{t}$H [6]). In the case of WH and ZH the MiNLO HVJ extension of POWHEG is used [7]. The description of the decay of the Higgs boson to four leptons is obtained using the JHUGEN generator [8]. In the case of WH, ZH and $t\bar{t}$H, the Higgs boson is allowed to decay to H$\to ZZ \to 2\ell$2X such that 4-lepton events where two leptons originate from the decay of associated Z, W bosons or top quarks are also taken into account in the simulation. Showering of parton-level events is done using PYTHIA8.209, and in all cases matching is performed by allowing QCD emissions at all energies in the shower and vetoing them afterwards according to the POWHEG internal scale. All samples are generated with the NNPDF 3.0 NLO parton distribution functions (PDFs) [9]. The list of Higgs signal samples and their cross sections are shown in Table 1.5.

Production of ZZ via quark-antiquark annihilation is generated at next-to-leading order (NLO) using POWHEG V2 [10] and PYTHIA8, with the same settings as for the Higgs signal. As this simulation covers a large range of ZZ invariant masses, dynamical

Process	Dataset Name	$\sigma \times BR(\times\epsilon_{\text{filter}})$
$gg \to H \to ZZ \to 4\ell$	/GluGluHToZZTo4L_M125_13TeV_powheg2_JHUgenV6_pythia8	12.18 fb
$qq \to Hqq \to ZZqq \to 4\ell qq$	/VBF_HToZZTo4L_M125_13TeV_powheg2_JHUgenV6_pythia8	1.044 fb
$q\bar{q} \to W^+H \to W^+ZZ \to 4\ell + X$	/WplusH_HToZZTo4L_M125_13TeV_powheg2-minlo-HWJ_JHUgenV6_pythia8	0.232 fb
$q\bar{q} \to W^-H \to W^-ZZ \to 4\ell + X$	/WminusH_HToZZTo4L_M125_13TeV_powheg2-minlo-HWJ_JHUgenV6_pythia8	0.147 fb
$q\bar{q} \to ZH \to ZZZ \to 4\ell + X$	/ZH_HToZZ_4LFilter_M125_13TeV_powheg2-minlo-HZJ_JHUgenV6_pythia8	0.668 fb
$gg \to ttH \to ttZZ \to 4\ell + X$	/ttH_HToZZ_4LFilter_M125_13TeV_powheg_JHUgen_pythia8	0.393 fb

Table 1.5: Higgs signal samples and cross sections.

Process	Dataset Name	$\sigma \cdot BR$
$qq \to ZZ \to 4\ell$	/ZZTo4L_13TeV_powheg_pythia8/[1]	1.256pb
$qq \to ZZ \to 4\ell$	/ZZTo4L_13TeV-amcatnloFXFX-pythia8/[1]	1.212pb
$gg \to ZZ \to 4e$	/GluGluToContinToZZTo4e_13TeV_MCFM701/[1]	0.00159pb
$gg \to ZZ \to 4\mu$	/GluGluToContinToZZTo4mu_13TeV_MCFM701/[1]	0.00159pb
$gg \to ZZ \to 4\tau$	/GluGluToContinToZZTo4tau_13TeV_MCFM701/[1]	0.00159pb
$gg \to ZZ \to 2e2\mu$	/GluGluToContinToZZTo2e2mu_13TeV_MCFM701/[1]	0.00319pb
$gg \to ZZ \to 2e2\tau$	/GluGluToContinToZZTo2e2tau_13TeV_MCFM701/[1]	0.00319pb
$gg \to ZZ \to 2\mu 2\tau$	/GluGluToContinToZZTo2mu2tau_13TeV_MCFM701/[1]	0.00319pb
$Z \to \ell\ell$ + jets	/DYJetsToLL_M-50_TuneCUETP8M1_13TeV-amcatnloFXFX-pythia8/[1]	6104pb
$Z \to \ell\ell$ + jets	/DYJetsToLL_M-10to50_TuneCUETP8M1_13TeV-amcatnloFXFX-pythia8/[1]	18610pb
$WZ \to 3\ell\nu$	/WZTo3LNu_TuneCUETP8M1_13TeV-powheg-pythia8/[1]	4.430pb
$t\bar{t}$	/TTJets_TuneCUETP8M1_13TeV-amcatnloFXFX-pythia8/[1]	815.96pb
$t\bar{t} \to 2\ell 2\nu 2b$	/TTTo2L2Nu_13TeV-powheg/[1]	87.31pb

[1] RunIISummer16MiniAODv2-PUMoriond17_80X_mcRun2_asymptotic_2016_TrancheIV_v6-v1

Table 1.6: Background Monte Carlo samples and cross sections.

QCD factorization and renormalization scales have been chosen, equal to m_{ZZ}.

The $gg \to ZZ$ process is simulated at leading order (LO) with MCFM [11, 12]. In order to match the $gg \to H \to ZZ$ transverse momentum spectra predicted by POWHEG at NLO, the showering for MCFM samples is performed with different PYTHIA8 settings, allowing only emissions up to the parton-level scale ("wimpy" shower).

Although not directly used to model data observations, additional MC samples of WZ, Drell-Yan+jets, $t\bar{t}$, and tribosons are generated using MadGraph5_aMCatNLO [13] either inclusively or merging several jet multiplicities, as detailed in the table. Table 1.6 summarizes the MC simulation datasets used for this analysis.

1.2.2.1 Pileup Reweighting

The MC samples are reweighted to match the pileup distribution measured in 2016 data. Scale factors are measured and applied to each event weight before histograms are filled and yields are calculated, based on the number of pileup vertices present in the event. The mean number of pileup vertices for data measured in 2016 is about 20. Figure **??** shows the distributions of the numbers of pileup vertices for data and MC before and after the events are reweighted.

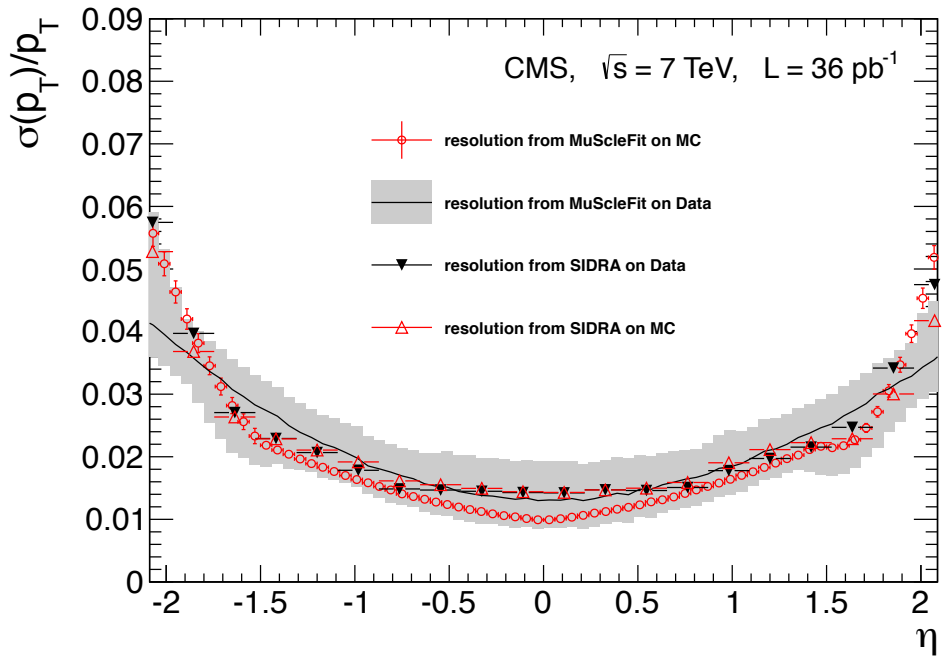

Figure 1.2: Number of pileup vertices before and after reweighted is applied.

Appendices

Appendix A

Production Cross Sections for Benchmark Signal Models

m_χ [GeV]	1	10	50	65	100	200	400	800	1000	1300
EFT_HHxx_scalar										
	0.10071E+01	0.99793E+00	0.60671E+00	0.48291E-04	0.22725E-05	0.11059E-06	0.36569E-08	0.40762E-10	0.64956E-11	0.51740E-12
EFT_HHxx_combined										
	0.15731E+01	0.15194E+01	0.34134E+00	0.41039E-04	0.10581E-04	0.16553E-05	0.14628E-06	0.40608E-08	0.85950E-09	0.96480E-10
EFT_HHxg5x										
	0.15735E+03	0.15594E+03	0.94804E+02	0.12990E-01	0.23075E-02	0.41820E-03	0.45743E-04	0.16734E-05	0.39327E-06	0.49769E-07
EFT_xdxHDHc										
Λ = 100 GeV	0.29530E+00	0.29067E+00	0.10540E+00	0.89849E-01	0.64959E-01	0.30639E-01	0.88644E-02	0.97986E-03	0.33847E-03	0.68674E-04
Λ = 1000 GeV	0.16306E-04	0.15508E-04	0.12088E-05	0.88288E-06	0.53312E-06	0.18046E-06	0.34918E-07	0.27514E-08	0.90662E-09	0.19313E-09
EFT_xgxFHDH										
	0.57027E+00	0.57001E+00	0.56025E+00	0.55337E+00	0.53270E+00	0.45792E+00	0.29777E+00	0.10288E+00	0.57444E-01	0.23260E-01

Table A.1: EFT production cross sections [pb]

m_χ [GeV]	m_S [GeV]								
1	0.21915E+01	0.20798E+01	0.19192E+01	0.18118E+01	0.16735E+01	0.52244E+01	0.41877E+01	0.28732E+01	0.18028E+01
10	0.17416E+01	0.17420E+01	0.18581E+01	0.17510E+01					0.17398E+01
50	0.39053E+00		0.38877E+00	0.38409E+00	0.37097E+00	0.12861E+01			0.39096E+00
150	0.24136E-05				0.38372E-05	0.21922E-04	0.42337E-03	0.57124E-04	0.11105E-04
500	0.34099E-08						0.49399E-08	0.25206E-06	0.36823E-06
1000	0.17012E-10							0.55260E-10	0.11067E-07

Table A.2: Scalar production cross sections [pb] corresponding to mass points in Table **??**

m_χ [GeV]	$m_{Z'}$ [GeV]										
1	0.26615E+01	0.27802E+01	0.33248E+01	0.32341E+01	0.26566E+01	0.23191E+01	0.10842E+01	0.18700E+00	0.11728E-01	0.17399E-07
10	0.21182E-01	0.74027E-01	0.32732E+01	0.32250E+01						0.17380E-07
50	0.36342E-03		0.12726E-01	0.31337E+00	0.21226E+01	0.20120E+01				0.17340E-07
150	0.55972E-05				0.56526E-02	0.18000E+00	0.67266E+00	0.18111E+00		0.16918E-07
500	0.80295E-08						0.36591E-04	0.10368E-01	0.10375E-01	0.13179E-07
1000	0.49387E-10							0.98079E-06	0.57596E-03	0.80146E-08

Table A.3: ZpBaryonic production cross sections [pb] corresponding to mass points in Table **??**

m_χ [GeV]	$m_{Z'}$ [GeV]									
1	0.61935E-02	0.63192E-02	0.82991E-02	0.11942E-01	0.19171E-01	0.21560E-01	0.16010E-01	0.64416E-02	0.56526E-02	0.58902E-02
10	0.58781E-02	0.58938E-02	0.82944E-02	0.11937E-01						0.58805E-02
50	0.10294E-03		0.77820E-04	0.15258E-04	0.12066E-01	0.12105E-01				0.10387E-03
150	0.28382E-06				0.83917E-05	0.72889E-03	0.65401E-02	0.68337E-03		0.29033E-06
500	0.34689E-09						0.43355E-06	0.87799E-04	0.28292E-05	0.36327E-09
1000	0.20703E-11							0.44782E-07	0.19974E-06	0.27001E-11

Table A.4: ZpHS production cross sections [pb] corresponding to mass points in Table **??**

m_{A^0} [GeV]	$m_{Z'}$ [GeV]							
300	42.386	45.097	35.444	26.07	18.942	11.778	7.4456	3.6446
400	5.8513	14.847	14.534	11.792	9.029	5.851	3.7819	1.8758
500		5.9605	8.4961	7.9575	6.5515	4.5063	3.0028	1.5235
600		1.5853	4.6972	5.4808	4.9946	3.7044	2.5694	1.3447
700			2.1092	3.4848	3.6766	3.0253	2.2023	1.1984
800			0.65378	1.9638	2.5511	2.4077	1.8689	1.0692

Table A.5: Zp2HDM production cross sections [pb] corresponding to mass points in Table **??**

References

[1] S. Alioli, P. Nason, C. Oleari, and E. Re. NLO vector-boson production matched with shower in POWHEG. *JHEP*, 07:060, 2008. arXiv:0805.4802, doi:10.1088/1126-6708/2008/07/060.

[2] Paolo Nason. A new method for combining NLO QCD with shower Monte Carlo algorithms. *JHEP*, 11:040, 2004. arXiv:hep-ph/0409146, doi:10.1088/1126-6708/2004/11/040.

[3] Stefano Frixione, Paolo Nason, and Carlo Oleari. Matching NLO QCD computations with parton shower simulations: the POWHEG method. *JHEP*, 11:070, 2007. arXiv:0709.2092, doi:10.1088/1126-6708/2007/11/070.

[4] E. Bagnaschi, G. Degrassi, P. Slavich, and A. Vicini. Higgs production via gluon fusion in the POWHEG approach in the SM and in the MSSM. *JHEP*, 02:088, 2012. arXiv:1111.2854, doi:10.1007/JHEP02(2012)088.

[5] Paolo Nason and Carlo Oleari. NLO Higgs boson production via vector-boson fusion matched with shower in POWHEG. *JHEP*, 02:037, 2010. arXiv:0911.5299, doi:10.1007/JHEP02(2010)037.

[6] Heribertus B. Hartanto, Barbara Jager, Laura Reina, and Doreen Wackeroth. Higgs boson production in association with top quarks in the POWHEG BOX. *Phys. Rev.*, D91(9):094003, 2015. arXiv:1501.04498, doi:10.1103/PhysRevD.91.094003.

[7] Gionata Luisoni, Paolo Nason, Carlo Oleari, and Francesco Tramontano. $HW^{\pm}$/HZ + 0 and 1 jet at NLO with the POWHEG BOX interfaced to GoSam and their merging within MiNLO. *JHEP*, 10:083, 2013. arXiv:1306.2542, doi:10.1007/JHEP10(2013)083.

[8] Yanyan Gao, Andrei V. Gritsan, Zijin Guo, Kirill Melnikov, Markus Schulze, and Nhan V. Tran. Spin determination of single-produced resonances at hadron colliders. *Phys. Rev. D*, 81:075022, 2010. arXiv:1001.3396, doi:10.1103/PhysRevD.81.075022.

[9] Richard D. Ball et al. Parton distributions for the LHC Run II. *JHEP*, 04:040, 2015. arXiv:1410.8849, doi:10.1007/JHEP04(2015)040.

[10] Paolo Nason and Giulia Zanderighi. W^+W^- , WZ and ZZ production in the POWHEG-BOX-V2. *Eur. Phys. J.*, C74(1):2702, 2014. arXiv:1311.1365, doi:10.1140/epjc/s10052-013-2702-5.

[11] John M. Campbell and R. K. Ellis. MCFM for the Tevatron and the LHC. *Nucl. Phys. Proc. Suppl.*, 205:10, 2010. arXiv:1007.3492, doi:10.1016/j.nuclphysbps.2010.08.011.

[12] John M. Campbell, R. Keith Ellis, and Ciaran Williams. Bounding the Higgs width at the LHC using full analytic results for $gg- > e^-e^+\mu^-\mu^+$. *JHEP*, 04:060, 2014. arXiv:1311.3589, doi:10.1007/JHEP04(2014)060.

[13] J. Alwall, R. Frederix, S. Frixione, V. Hirschi, F. Maltoni, O. Mattelaer, H. S. Shao, T. Stelzer, P. Torrielli, and M. Zaro. The automated computation of tree-level and next-to-leading order differential cross sections, and their matching to parton shower simulations. *JHEP*, 07:079, 2014. arXiv:1405.0301, doi:10.1007/JHEP07(2014)079.